2005

The Nature of Radio Continuum Emission at Very Low Metallicity: VLA Observations of I Zw 18

John M Cannon, *Macalester College*
E. D. Skillman
L. van Zee
F. Walter

The Astrophysical Journal, 621:L21–L24, 2005 March 1

THE NATURE OF RADIO CONTINUUM EMISSION AT VERY LOW METALLICITY: VERY LARGE ARRAY OBSERVATIONS OF I Zw 18

John M. Cannon and Fabian Walter
Max-Planck-Institut für Astronomie, Königstuhl 17, D-69117 Heidelberg, Germany; cannon@mpia.de, walter@mpia.de
Evan D. Skillman
Department of Astronomy, University of Minnesota, 116 Church Street SE, Minneapolis, MN 55455; skillman@astro.umn.edu
and
Liese van Zee
Department of Astronomy, Indiana University, 727 East Third Street, Bloomington, IN 47405; vanzee@astro.indiana.edu
Received 2004 December 13; accepted 2005 January 20; published 2005 February 3

ABSTRACT

We present the first resolved study of the radio continuum properties of I Zw 18, the dwarf galaxy with the lowest known nebular metal abundance in the local universe. New Very Large Array radio continuum images at 20 and 3.6 cm are compared to various *Hubble Space Telescope* images, and we find a striking morphological similarity between high-resolution Hα and short-wavelength radio continuum emission, especially in the Hα shell in the northwest region. We separate thermal and nonthermal components of the emission and find a large synchrotron halo surrounding the galaxy. Comparison between Hα and X-band fluxes suggests that the emission at 3.6 cm is dominated by thermal processes; an additional synchrotron component dominates the flux at 20 cm and produces a modest fraction of the detected flux at 3.6 cm. The fluxes of three of the four major emission peaks show a mix of thermal and nonthermal processes, while one shows a nearly flat spectral index. The strong synchrotron component argues for active star formation throughout the disk for at least the last ~30 Myr. These sensitive observations provide a new, detailed view of the nature of radio continuum emission in the very low metallicity interstellar medium. Comparing with the literature, the role of metallicity in the evolution of radio continuum emission seems to be secondary to other factors such as the recent star formation history and the presence or absence of outflows from star formation regions.

Subject headings: galaxies: dwarf — galaxies: evolution — galaxies: individual (I Zw 18) — radio continuum: galaxies

1. INTRODUCTION

With the lowest nebular metallicity known in the local universe [(O/H) ~ 0.02 $(O/H)_{\odot}$; Skillman & Kennicutt 1993], I Zw 18 plays a key role in the study of galaxy evolution. Understanding the nature of the star-forming fragments predicted at high redshift requires a detailed study of nearby potentially "young" galaxies. Estimates of the age of the stellar population in I Zw 18 based on single-star photometry suggest an age of less than 1 Gyr (e.g., Hunter & Thronson 1995; Aloisi et al. 1999; Östlin 2000; Izotov & Thuan 2004).

An alternative probe of the unobscured, recent ($\lesssim$30 Myr) star formation in a galaxy can be obtained with radio continuum observations. Three types of radio continuum emission are seen in local star-forming galaxies (see Condon 1992 for a detailed review). First, thermal free-free emission (characterized by a nearly flat spectral index, $\alpha \sim -0.1$, where $S_{\nu} \sim \nu^{\alpha}$) is proportional to the total Lyman continuum flux and hence can be used as an accurate star formation rate estimator. Second, nonthermal synchrotron emission, produced in supernova (SN) explosions and remnants, shows a more negative spectral index ($-1.2 \lesssim \alpha \lesssim -0.4$). Finally, free-free absorption can occur in young, dense, heavily embedded clusters that show an inverted spectrum ($\alpha > 0.0$; Turner et al. 1998; Kobulnicky & Johnson 1999; Johnson & Kobulnicky 2003). Distinguishing between these emission mechanisms allows one to constrain the ages of the emitting components: inverted sources are very young (ages ~10^5–10^6 yr; Johnson et al. 2001); thermal regions have ages comparable to those of H II regions ($\lesssim$10 Myr); and synchrotron radiation dominates in regions older than this.

Considering the amount of observational attention that I Zw 18 has received, it is somewhat surprising that no detailed investigation of its radio continuum properties exists in the literature. There have been two previously published radio continuum detections, but both have been extracted from spectral line observations (Lequeux & Viallefond 1980; van Zee et al. 1998). In order to study the nature of radio continuum emission at the lowest available nebular metallicity, we have obtained sensitive Very Large Array (VLA)[1] observations of I Zw 18. We compare these data to *Hubble Space Telescope* (*HST*)[2] images of the stellar and nebular emission. Throughout this Letter, we adopt a distance of 12.6 Mpc for I Zw 18 (Östlin 2000); however, most of our results (spectral indices, comparison to *HST* imaging) do not require a tightly constrained distance estimate.

2. OBSERVATIONS AND DATA REDUCTION

2.1. *VLA Radio Continuum Data*

VLA radio continuum imaging was obtained using the A, B, and C arrays on 2003 August 3, 2004 January 20, and 2004 April 20 (total on-source integration time = 15.1 hr) for program AC681. All reductions were performed using the AIPS package. First, interference and bad data were removed. Flux, gain, and phase calibrations were then applied, derived from

[1] The VLA is operated by the National Radio Astronomy Observatory, which is a facility of the National Science Foundation operated under cooperative agreement by Associated Universities, Inc.

[2] Based on observations with the NASA/ESA *HST*, obtained at the Space Telescope Science Institute, which is operated by the Association of Universities for Research in Astronomy, Inc., under NASA contract NAS5-26555.

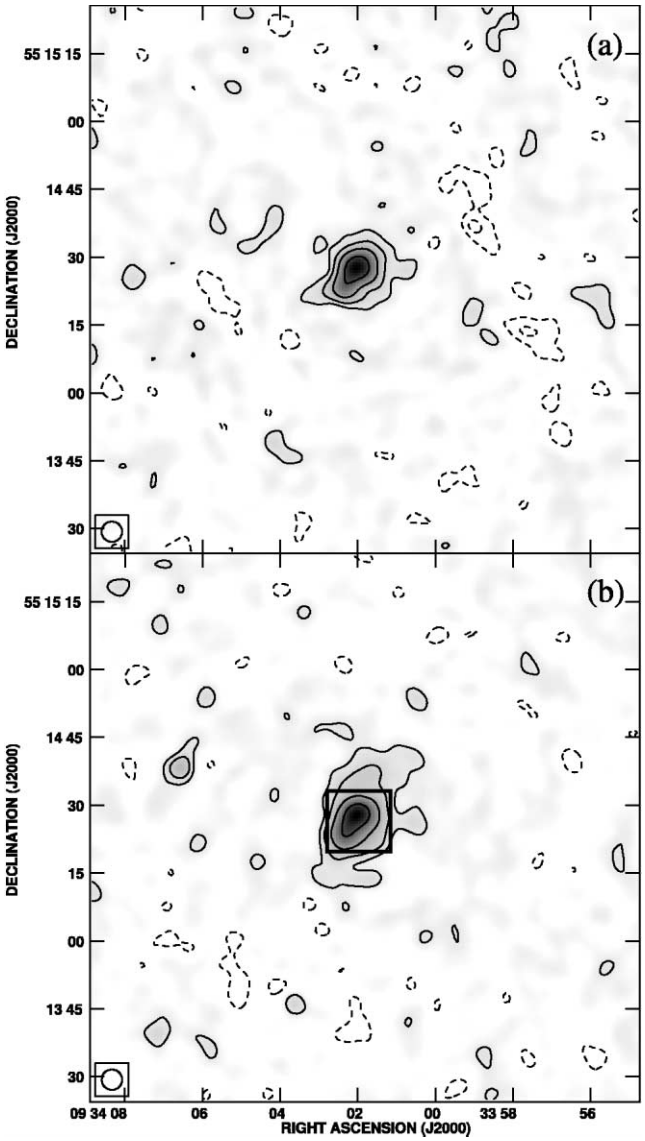

FIG. 1.—Low-resolution (*a*) X-band and (*b*) L-band images of I Zw 18, overlaid with contours at the −4, −2, 2, 4, 8, and 16 σ levels (X band: 1 σ = 12 μJy beam^{-1}; L band: 1 σ = 19 μJy beam^{-1}). The beam size is 4.″5 × 4.″5 and is shown at the bottom left. The black box in (*b*) outlines the approximate field of view shown in Figs. 2 and 3. Note that the diffuse emission is more spatially extended at 20 cm than at 3.6 cm.

observations of 1331+305 (3C 286; primary calibrator) and 0921+622 (secondary calibrator). The L-band (20 cm) and X-band (3.6 cm) observations were obtained in two arrays, and these *u*-*v* databases were concatenated. The calibrated *u*-*v* data were then imaged and cleaned to produce matched-beam images at each frequency that balanced resolution and sensitivity. We analyze a set of "high"-resolution (L band: beam = 2.″18 × 2.″01, rms = 11.6 μJy beam^{-1}; X band: beam = 2.″17 × 2.″07, rms = 7.4 μJy beam^{-1}) and a set of "low"-resolution (beam = 4.5″, L-band rms = 19 μJy beam^{-1}, X-band rms = 12 μJy beam^{-1}) images.

2.2. *HST Imaging*

We compare our radio observations to archival *HST* observations of I Zw 18 from programs GO-5434 (PI: R. J. Dufour), GO-6536 (PI: E. D. Skillman), and GO-9400 (PI: T. X. Thuan). The detailed handling of the data from programs 6536 and 5434 are presented in Cannon et al. (2002). We use the same narrowband Hα image presented in that work for analysis here [total Hα flux = (3.26 ± 0.3) × 10^{-13} ergs s^{-1} cm^{-2}, implying a current star formation rate of ~0.05 $M_\odot$ yr^{-1} (Kennicutt et al. 1994)]. From program 9400, we use an *HST*/Advanced Camera for Surveys (ACS) F555W image for comparison with the stellar continuum. Based on the positions of *HST* Guide Stars in the ACS field and the agreement of the radio and Hα peaks, we conservatively estimate the uncertainty in the coordinate solution to be better than 0.″5 rms.

3. THE NATURE OF RADIO CONTINUUM EMISSION

3.1. *Global Flux Measurements*

In Figure 1 we present the low-resolution images overlaid with contours at various levels. We measure global flux densities (by integrating continuous emission surrounding the galaxy after blanking at the 3 σ level) at the L and X bands of 1.79 ± 0.18 and 0.78 ± 0.08 mJy, respectively, corresponding to a global spectral index of −0.46 ± 0.06 (see Table 1). The continuum emission is more spatially extended at 20 cm than at 3.6 cm (although the latter data are significantly more sensitive); indeed, emission above the 3 σ level is detected out to ~12″ (deconvolved) northwest of the emission peak at the L band (corresponding to a linear distance of ~730 pc at the adopted distance), but only to ~7.″5 at the X band. As argued in the next section, this is the result of a synchrotron halo surrounding the system.

TABLE 1
PROPERTIES OF RADIO CONTINUUM EMISSION IN I ZW 18

Parameter	I Zw 18 SE	I Zw 18 NW-A	I Zw 18 NW-B	I Zw 18 NW-C	I Zw 18 Total Galaxy
R.A. (J2000)	09 34 02.36	09 34 02.10	09 34 01.85	09 34 01.82	09 34 02.0
Decl. (J2000)	+55 14 23.10	+55 14 28.06	+55 14 26.00	+55 14 29.06	+55 14 28
Aperture radius (arcsec)	1.75	1.5	1.1	1.1	…
S_L (mJy)	0.17 ± 0.02	0.20 ± 0.02	0.050 ± 0.005	0.079 ± 0.008	1.79 ± 0.18
S_X (mJy)	0.11 ± 0.01	0.12 ± 0.01	0.047 ± 0.005	0.050 ± 0.005	0.78 ± 0.08
α ($S_\nu \sim \nu^\alpha$)	−0.27 ± 0.06	−0.29 ± 0.06	−0.04 ± 0.06	−0.26 ± 0.06	−0.46 ± 0.06
Hα flux (10^{-14} ergs s^{-1} cm^{-2})	7.7 ± 0.8	7.8 ± 0.8	1.3 ± 0.2	2.9 ± 0.3	32.6 ± 3.3

NOTES.—Units of right ascension are hours, minutes, and seconds, and units of declination are degrees, arcminutes, and arcseconds. See Figs. 1 and 2 for positions. The central positions of the radio continuum emission peaks are derived from Gaussian fitting. The coordinates of the I Zw 18 system are taken from the NASA Extragalactic Database.

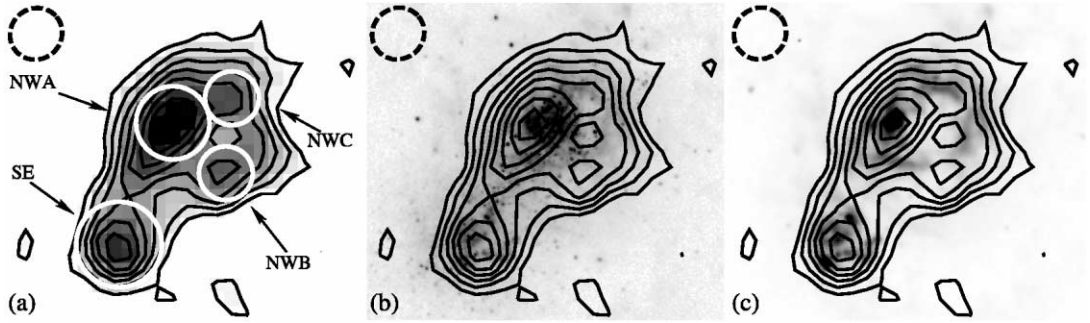

FIG. 2.—High-resolution X-band emission contours at the −3, 3, 4.5, 6, 7.5, 9, 10.5, 12, and 13.5 σ levels (1 σ = 7.4 μJy beam^{-1}), superposed (*a*) on a gray-scale image of the emission, (*b*) on an *HST*/ACS F555W (*V*) image, and (*c*) on an *HST*/WFPC2 F656N (continuum-subtracted Hα) image. Labels and the white circles in (*a*) denote the apertures used to measure fluxes of individual peaks in the radio continuum and in Hα (see § 3 and Table 1). The beam size is 2.″17 × 2.″07 and is shown at upper left. The field of view (with north up and east to the left) is ~0.9 × 0.8 kpc at the adopted distance of 12.6 Mpc.

3.2. *Thermal versus Nonthermal Decomposition*

Since the thermal radio continuum luminosity is proportional to the total photoionization rate, there exists a well-defined relation between radio continuum luminosity and other direct star formation rate indicators (e.g., Hα emission). In systems with little extinction in the optical, this relation can be used to estimate the expected thermal fraction of detected radio continuum emission. In I Zw 18, the low detected extinctions ($A_V \lesssim 0.5$ mag; see Cannon et al. 2002) imply that Hα provides a nearly complete census of the ongoing star formation.

We can estimate the expected thermal components at each frequency using the relations presented in Caplan & Deharveng (1986). For a purely thermal radio continuum source in the absence of extinction, the Hα flux and the flux density at a given frequency are related via

$$\frac{j_{\mathrm{H}\alpha}}{j_\nu} = \frac{8.67 \times 10^{-9} T^{-0.44}}{10.811 + 1.5 \ln T - \ln \nu}, \quad (1)$$

where $j_{\mathrm{H}\alpha}$ is the flux at Hα in units of ergs s^{-1} cm^{-2}, j_ν is the flux density at the given frequency in units of janskys, T is the electron temperature in units of 10^4 K, and ν is the observed frequency in units of gigahertz. We adopt an intermediate electron temperature from Skillman & Kennicutt (1993) of 18,500 K for the entire galaxy. Using the global Hα flux measured from the *HST* image (see Table 1), we expect flux densities of 0.47 mJy at the X band and 0.56 mJy at the L band. Comparison with the measured X-band value of 0.78 mJy suggests that more than half of the 3.6 cm emission is thermal; conversely, only ~30% of the emission at the L band is expected to be thermal.

Given this expected value for thermal emission at 20 cm, >70% of the detected emission can be attributed to a synchrotron component. If this emission has a characteristic synchrotron spectral index ($\alpha = -0.8$), then this implies a synchrotron contribution to the detected flux at X band of 0.29 mJy. This value can be compared with the difference between total and (predicted) thermal fluxes, 0.31 mJy; the agreement suggests that such a synchrotron component fits the data quite well.

3.3. *Properties of Individual Radio Emission Peaks*

We present higher resolution images of the radio continuum emission from I Zw 18 in Figures 2 and 3, as well as overlays of the emission on *HST* Hα and *V*-band images. We resolve the emission into four distinct peaks at this resolution. Examining these images, there is a striking correlation between Hα and radio continuum emission at this sensitivity level; in all areas of high surface brightness Hα emission, strong radio continuum emission is prevalent. Note also that the radio continuum emission closely follows the diffuse Hα shell morphology in the northwest region.

The total flux densities of the individual peaks were measured using identical apertures the size of the beam or larger, centered on the peaks in the X-band image (see Fig. 2 and Table 1). The individual radio continuum peaks are found to have a mix of thermal and nonthermal spectral indices. Three of the sources (I Zw 18 SE, NW-A, NW-C) have spectral indices $\alpha \sim -0.27$, implying a mix of thermal and nonthermal components. I Zw 18 NW-B, however, is consistent with nearly purely thermal emission ($\alpha = -0.04 \pm 0.06$).

Sources I Zw 18 SE and NW-A are clearly associated with

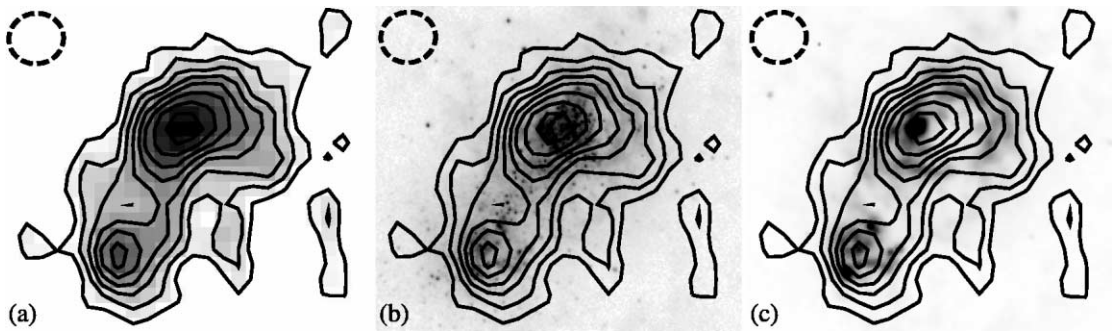

FIG. 3.—Same as Fig. 2, but for the L-band high-resolution data (1 σ = 11.6 μJy beam^{-1}). Comparing to the X-band emission at similar resolution, it is clear that the individual emission peaks are less well defined; we interpret this as the result of the additional synchrotron component at the L band. The beam size is 2.″18 × 2.″04 and is shown at upper left.

collections of the high surface brightness H II regions of the galaxy. The high (aperture-integrated) Hα equivalent widths found in Cannon et al. (2002) imply strong active star formation, while their nonthermal radio continua suggest that the areas are also rich in massive star feedback via SN explosions and remnants. This suggests that the star formation intensity was strong ~20–30 Myr ago, as well as at the present epoch. This is in good agreement with the results of resolved stellar population analysis, in which recent investigations have found a star formation rate that was elevated during the last 10–100 Myr compared to that at present (Aloisi et al. 1999; Östlin 2000; Izotov & Thuan 2004).

4. DISCUSSION AND CONCLUSIONS

The nature of radio continuum emission at very low metallicities is only beginning to be explored. Comparing our results with those on the second-most metal-poor galaxy known, SBS 0335−052 (Hunt et al. 2004), we find that both systems have a mix of nonthermal and thermal components, indicative of active massive star formation over the last ~30 Myr. However, the radio spectrum of SBS 0335−052 has a thermal component that manifests itself in considerable absorption at the L band and a radio turnover between 1.4 and 4.8 GHz. While the present data set has fewer frequencies, we would be sensitive to a similar spectral turnover in I Zw 18 (as this would result in positive, rather than negative, spectral indices between 3.6 and 20 cm).

The differences in the radio continuum properties of I Zw 18 and SBS 0335−052 are most easily explained as the results of the more vigorous star formation event that is underway in the latter. I Zw 18 appears to be undergoing star formation in discrete stellar clusters and H II regions (see Table 1 for Hα luminosities of the radio emission peaks studied here, and Cannon et al. 2002 for those of other clusters), and infrared imaging (e.g., Östlin 2000; Östlin & Mouchine 2005) does not suggest embedded regions that would be able to give rise to "super star clusters" (SSCs; see O'Connell 2004 for a recent review of SSC properties). SBS 0335−052, on the other hand, hosts multiple SSCs (Thuan et al. 1997) and regions of exceptionally high extinction and embedded star formation for a very metal-poor galaxy (Hunt et al. 2001; Plante & Sauvage 2002). Given that complex (and often inverted) spectral indices typically arise from such regions (Turner et al. 1998; Kobulnicky & Johnson 1999; Johnson & Kobulnicky 2003), it is perhaps not surprising that the radio spectra of I Zw 18 and SBS 0335−052 appear to differ.

To summarize, we have detected thermal and nonthermal emission in I Zw 18, including a synchrotron halo. This low-metallicity, low-dust system shows a radio continuum spectrum between 20 and 3.6 cm that is typical of star-forming dwarf galaxies; however, the radio properties differ markedly from those found in the second-most metal-poor galaxy, SBS 0335−052. Although the sample is small, the variety of radio continua found at very low metallicities suggests that there is not a strong metallicity dependence for the production of radio continuum emission. Indeed, it is not necessary that one should exist; thermal continua are produced by stars that have formed, while nonthermal continua are typically the result of the evolution of massive stars. While there certainly exist differences in the way that the stars form at different metallicities, once the stars have formed, radio continuum emission appears to be ubiquitous (although complex and dependent on other factors) in massive star formation regions regardless of metallicity.

The authors would like to thank Chip Kobulnicky for helpful discussions during the planning stages of this project and the anonymous referee for helpful comments.

REFERENCES

Aloisi, A., Tosi, M., & Greggio, L. 1999, AJ, 118, 302
Cannon, J. M., Skillman, E. D., Garnett, D. R., & Dufour, R. J. 2002, ApJ, 565, 931
Caplan, J., & Deharveng, L. 1986, A&A, 155, 297
Condon, J. J. 1992, ARA&A, 30, 575
Hunt, L. K., Dyer, K. K., Thuan, T. X., & Ulvestad, J. S. 2004, ApJ, 606, 853
Hunt, L. K., Vanzi, L., & Thuan, T. X. 2001, A&A, 377, 66
Hunter, D. A., & Thronson, H. A. 1995, ApJ, 452, 238
Izotov, Y. I., & Thuan, T. X. 2004, ApJ, 616, 768
Johnson, K. E., & Kobulnicky, H. A. 2003, ApJ, 597, 923
Johnson, K. E., Kobulnicky, H. A., Massey, P., & Conti, P. S. 2001, ApJ, 559, 864
Kennicutt, R. C., Jr., Tamblyn, P., & Congdon, C. E. 1994, ApJ, 435, 22
Kobulnicky, H. A., & Johnson, K. E. 1999, ApJ, 527, 154
Lequeux, J., & Viallefond, F. 1980, A&A, 91, 269
O'Connell, R. W. 2004, in ASP Conf. Ser. 322, The Formation and Evolution of Massive Young Star Clusters, ed. H. J. G. L. M. Lamers, L. J. Smith & A. Nota (San Francisco: ASP), 551
Östlin, G. 2000, ApJ, 535, L99
Östlin, G., & Mouchine, M. 2005, A&A, in press (astro-ph/0411217)
Plante, S., & Sauvage, M. 2002, AJ, 124, 1995
Skillman, E. D., & Kennicutt, R. C., Jr. 1993, ApJ, 411, 655
Thuan, T. X., Izotov, Y. I., & Lipovetsky, V. A. 1997, ApJ, 477, 661
Turner, J. L., Ho, P. T. P., & Beck, S. C. 1998, AJ, 116, 1212
van Zee, L., Westpfahl, D., Haynes, M. P., & Salzer, J. J. 1998, AJ, 115, 1000